

Limit state equation and failure pressure prediction model of pipeline with complex loading

Received: 14 September 2023

Accepted: 8 May 2024

Published online: 25 May 2024

Ming-ming Sun^{1,2,3}, Hong-yuan Fang^{1,2,3}✉, Nian-nian Wang^{1,2,3},
Xue-ming Du^{1,2,3}, Hai-sheng Zhao^{4,5} & Ke-Jie Zhai^{1,2,3}

Assessing failure pressure is critical in determining pipeline integrity. Current research primarily concerns the buckling performance of pressurized pipelines subjected to a bending load or axial compression force, with some also looking at the failure pressure of corroded pipelines. However, there is currently a lack of limit state models for pressurized pipelines with bending moments and axial forces. In this study, based on the unified yield criterion, we propose a limit state equation for steel pipes under various loads. The most common operating loads on buried pipelines are bending moment, internal pressure, and axial force. The proposed limit state equation for intact pipelines is based on a three-dimensional pipeline stress model with complex load coupling. Using failure data, we investigate the applicability of various yield criteria in assessing the failure pressure of pipelines with complex loads. We show that the evaluation model can be effectively used as a theoretical solution for assessing the failure pressure in such circumstances and for selecting appropriate yield criteria based on load condition differences.

Due to their large capacity, high bearing capacity, and low environmental impact, steel pipelines are widely used as a safe and cost-effective material for long-distance water diversion, urban heating, and transportation of oil, gas, and other materials^{1–3}. Internal pressure determines the size of the pipeline and the efficiency with which material is transported^{4–6}. Currently, the largest diameter of a pressurized pipe is 1200 mm, and as pipeline transportation distance increases, so does the operating pressure, which can reach more than 10 MPa. For crude oil and other mediums with high viscosity and freezing points, the transportation pressure can reach 20 MPa to ensure normal transportation. We can infer that assessing failure pressure is critical in determining pipeline integrity.

During operation, buried pipelines are subjected to combined loads such as axial force, internal pressure, and bending moment^{7–9}.

Internal pressure in buried pipelines is primarily caused by the internal transport medium, with axial force resulting from temperature differences during laying and operation. Geotechnical disturbances may cause axial forces within the pipeline. For example, when pipelines cross a slope, the pipelines at the bottom withstand axial compression while those at the top withstand axial tension¹⁰. The Poisson effect is another type of axial force in materials. Because of the pressure inside the pipeline, radial expansion will attempt to shorten the pipeline's axial length. Pipelines may also experience bending moments due to soil movement caused by landslides, settlements, frost heave, earthquakes, foundation subsidence, and debris flows.

In this case, mechanical model analysis and bearing capacity evaluation of intact pipelines are the foundation for evaluating pipeline system integrity¹¹. Taylor et al.¹² demonstrated that an additional

¹School of Water Conservancy and Transportation, Zhengzhou University, Zhengzhou 450001, China. ²National Local Joint Engineering Laboratory of Major Infrastructure Testing and Rehabilitation Technology, Zhengzhou 450001, China. ³Collaborative Innovation Center of Water Conservancy and Transportation Infrastructure Safety, Zhengzhou 450001, China. ⁴State Key Laboratory of Coastal and Offshore Engineering, Dalian University of Technology, Dalian 116024, China. ⁵School of Hydraulic Engineering, Faculty of Infrastructure Engineering, Dalian University of Technology, Dalian 116024, China.

✉ e-mail: fanghongyuan1982@163.com

bending load reduced the failure pressure. Similar conclusions could be drawn for pipelines that could withstand axial forces^{13,14}. Therefore, assessing failure pressure solely based on internal pressure is limited, and it is necessary to examine the burst pressure of pipelines carrying complex loads.

According to reports, there is little literature on the integrity assessment of pipelines carrying complex loads. Early research focused on determining the bearing capacity of pipelines under two types of loads: axial force and internal pressure. Some studies^{15–22} referred to the research project of the Southwest Research Institute (SwRI) from the 1990s. Other references^{23–28} discussed the “reliability of corroded pipes” in the Joint Industry Projects (JIP) developed by DET NORSKE VERITAS (DNV). DNV’s method modifies the failure pressure model by including the stress factor H_1 . Without safety factors, the failure pressure p_f of an intact pipeline is calculated as follows:

$$p_f = \frac{2t\sigma_u}{D_e - t} H_1 \quad (1)$$

$$H_1 = 2 \left(1 + \frac{\sigma_L}{\sigma_u} \right) \quad (2)$$

Based on the above formulae, D_e is the diameter, t is the wall thickness, σ_L is the axial stress, and σ_u is the tensile strength. The above model is appropriate as corrosion defects can withstand compressive stress. However, increasing longitudinal stresses in the corrosion region ($\sigma_L < 0.25\sigma_u$) significantly decreases prediction accuracy²⁹.

Zhao et al.³⁰ proposed a prediction model for determining the burst pressure of a pipeline under axial load. However, this model assumes that the pipe section is subjected to the same axial stress, so it does not apply to the uneven axial stress caused by the bending moment. Zhou et al.³¹ discovered that axial stress reduced failure pressure and developed a vertical strain-based prediction formula. However, it is only applied to intact pipelines or pipelines with minor defects. Chen et al.³² first proposed a semi-empirical formula for calculating the failure pressure of pipelines subjected to internal pressure and axial tension, improving the theory of evaluating pipelines’ bearing capacity under complex loads. However, this method does not consider bending moment loads, and there is a need to confirm its accuracy for pipelines with other defect types.

Researchers have proposed more complex failure pressure assessment schemes to address the shortcomings of existing evaluation models. Chauhan and Swankee³³ and Liu et al.³⁴ proposed interactive charts to estimate the residual strength of pipelines under external loads. However, this method does not apply to pipelines with bending moments and axial forces. Heitzer³⁵ presented a mathematical programming formulation and used a numerical procedure to analyze pipeline plastic collapse under internal pressure and axial force. Benjamin³⁶ and Bruère et al.³⁷ proposed an approach to assess failure pressure that considers the impact of axial compressive force. Arumugam et al.³⁸ utilized the FE method to determine the bearing capacity of colony corrosion defects under compressive load and internal pressure. Zhang and Zhou³⁹ proposed an artificial neural network-based model for assessing the internal pressure bearing capability of pipelines subjected to axial force. Shuai et al.⁴⁰ applied finite element analysis to investigate the buckling bearing capacity of pipelines under axial compressive loading and internal pressure. Konosu and Mukaimachi⁴¹ put forward a plastic collapse assessment procedure for pressurized vessels with bending moments. Mohd et al.⁴² investigated the same pipeline case.

The FE method and failure tests determine the residual bearing capacity of pressurized pipelines with bending or multiple external loads. Mondal and Dhar²⁹ applied the finite element method to model marine pipelines and assess their structural integrity. Chegeni et al.⁴³ analyzed the effect of corrosion damage on the bearing capacity of

Table 1 | Calculation equation of failure pressure

case	additional load	principal stress	judging condition	Calculation equation
Case 1	positive	$\sigma_1 = \sigma_L$, $\sigma_2 = \sigma_h$, $\sigma_3 = 0$.	$\sigma_2 \leq \frac{\sigma_1 + \sigma_3}{2}$	$\left(\frac{1}{2} - \frac{b}{1+b}\right) \frac{p}{p_0} + \frac{\sum(\sigma_L)}{\sigma_u} = 1$
Case 2			$\sigma_2 > \frac{\sigma_1 + \sigma_3}{2}$	$\left(\frac{1}{2(1+b)} + \frac{b}{b+1}\right) \frac{p}{p_0} + \frac{1}{1+b} \frac{\sum(\sigma_L)}{\sigma_u} = 1$
Case 3		$\sigma_1 = \sigma_h$, $\sigma_2 = \sigma_L$, $\sigma_3 = 0$	-	$\frac{1}{1+b} \left(1 + \frac{b}{2}\right) \frac{p}{p_0} + \frac{b}{1+b} \frac{\sum(\sigma_L)}{\sigma_u} = 1$
Case 4	negative	$\sigma_1 = \sigma_h$, $\sigma_2 = 0$, $\sigma_3 = \sigma_L$	$\sigma_2 \leq \frac{\sigma_1 + \sigma_3}{2}$	$\left(1 - \frac{1}{2(1+b)}\right) \frac{p}{p_0} + \frac{1}{1+b} \frac{\sum(\sigma_L)}{\sigma_u} = 1$
Case 5			$\sigma_2 > \frac{\sigma_1 + \sigma_3}{2}$	$\left(\frac{1}{b+1} - \frac{1}{2}\right) \frac{p}{p_0} + \frac{\sum(\sigma_L)}{\sigma_u} = 1$
Case 6		$\sigma_1 = \sigma_h$, $\sigma_2 = \sigma_L$, $\sigma_3 = 0$	-	$\left(1 - \frac{b}{2(1+b)}\right) \frac{p}{p_0} + \frac{b}{1+b} \frac{\sum(\sigma_L)}{\sigma_u} = 1$

σ_1 , σ_2 , and σ_3 represent three types of principal stresses; σ_h and σ_L respectively denote circumferential and axial stresses; σ_u represents the tensile strength; p is the internal pressure load; p_0 denotes the ultimate bearing capacity of the internal pressure (only the internal pressure load is applied); and b is the yield criterion parameter.

pressurized pipelines under bending moment loads. Gao et al.⁴⁴ investigated the bending bearing capacity of pipelines carrying multiple loads. Similar studies were also conducted by ref. 29,45,46. Luigino et al.⁴⁷ described the key findings of the HOTPIPE project, which aimed to determine the bending moment capacity. Ozkan and Mohareb^{48,49} examined moment resistance through finite element modeling and full-scale experiments. Smith and Grigory¹⁷ proposed global buckling failure envelopes for pipelines with combined stresses. Roy et al.²² put forward a theoretical method to assess the integrity of pipelines with multiple loads. Agarwal⁵⁰ conducted a parametric study of pipelines with bending moment and pull force and proposed an optimization method for thickness distribution around them.

According to the literature review, the current research primarily concerns the buckling performance of pressurized pipelines subjected to a bending load or axial compression force. Some studies looked at the failure pressure of corroded pipelines using individual bending moments or axial compressive forces. However, there is currently no limit state model for pressurized pipelines with bending moments and axial forces.

This study presents the limit state equation of pipelines with complex loads based on the unified yield criterion (UYC) theory. This equation can calculate the failure pressure of intact pipelines under multiple or individual external loads (e.g., bending moment, axial compressive force, axial tensile force, and internal pressure). Moreover, this study combines the full-scale pressurized pipeline burst test with axial force to clarify the pipeline’s failure mechanism with complex loads. As combined with the burst test data, the accuracy of the limit state equation is verified.

Results

The limit state equation of pipeline with complex loading

Table 1 summarizes the limit state equations of pipelines under various conditions that can be utilized to solve the burst pressure with different yield criteria.

Analysis of experimental results

Figure 1 depicts photographs of intact pipeline explosion failures. The middle lower part of the pipeline burst, immediately tearing adjacent pipe walls, forming a burst opening, and causing noticeable bulging at the failure site.

As shown in Fig. 2a, the wall thickness distribution varied significantly in the circumferential direction while fluctuating minimally in the axial. The lower part of the pipeline in the circumferential direction of 252–324° had the smallest wall thickness, with an average

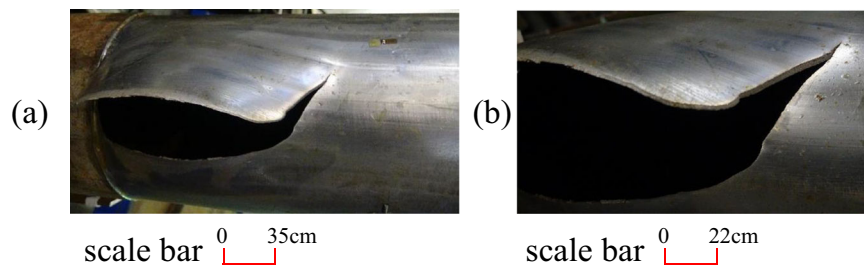


Fig. 1 | Failure modes of intact pipelines. a, b Global and partial failure diagrams of the pipeline test, respectively. The location of the pipeline burst failure exhibited significant expansion and shear failure under internal pressure.

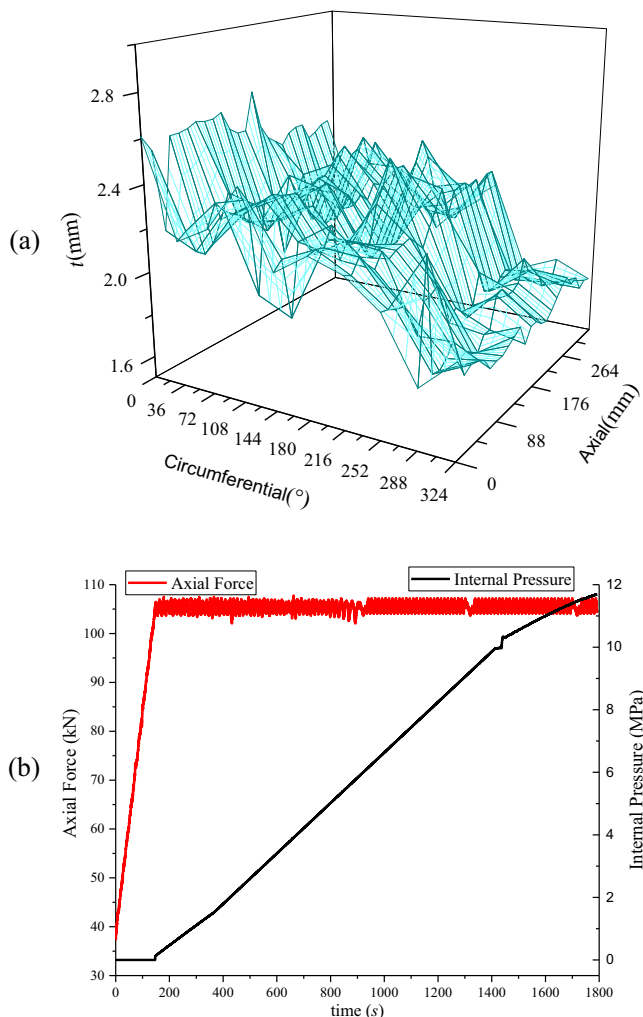


Fig. 2 | Test pipeline data. a Geometry distribution of wall thickness. The figure shows the difference between the circumferential and axial distributions of pipeline wall thickness. The pipeline's average wall thickness was 2.113 mm. Wall thickness had an average variance of 0.095 in the axial direction and 0.238 in the circumferential direction. In this case, the difference in wall thickness in the circumferential direction was more significant. In the circumferential direction, the wall thickness values within the 324° to 36° range were relatively large (average 2.49 mm). In contrast, the wall thickness values within the 252° to 324° range were relatively small (average of 1.81 mm). **b** Test loading curve. The load curve of the test depicts the various types and values of loads the pipeline could withstand at any loading time. Within 0–147 s, the internal pressure (0 MPa) remained constant while the axial load gradually increased from 37.5 kN to 105.5 kN. From 147 s to 1800 s, the axial load (105.5 kN) remained constant, while internal pressure increased until the pipeline failed. The pipeline's failure loads included an axial tension force of 68 kN and an internal pressure of 11.6 MPa.

of 1.81 mm, making it the most vulnerable to damage. The actual blasting position was in the middle and lower half of the 270° circumferential direction, which confirmed the wall thickness measurement results.

Figure 2b depicts the loading curve of an intact pipeline. Given that the loading device's unloaded gravity was 37.5 kN, it was initially loaded to 37.5 kN to eliminate its impact. Then, the axial force was increased to $37.5 + 68 = 105.5$ kN to simulate the increase in axial force caused by temperature differences. After being loaded to 105.5 kN, the axial force remained constant, and internal pressure was applied. The failure pressure for a pipeline explosion was 11.6 MPa.

Figure 3 presents the strain curve with axial force and internal pressure, while Fig. 4b depicts the strain gauge arrangement. The axial force load, followed by the internal pressure load, was 0–147 s. Accordingly, during axial force loading, the pipeline primarily experienced axial tensile deformation, while the circumferential measuring points R1–R12 generated compressive strain via Poisson's action. After the axial force loading was completed, internal pressure was applied, and the circumferential strain increased significantly. Figure 3a shows that the initial stage of internal pressure loading (147–600 s) ranged from 0 MPa to 3.4 MPa. The strain growth rate in R1–R12 was roughly the same, and the pipeline expanded uniformly. During the later loading stage, as the internal pressure exceeded 3.4 MPa, the strain change rate at each measuring point began to differ due to concentrated deformation at the failure site. The measuring point R11, located at the burst position, had the most significant strain growth rate and value. As the pipeline was about to burst approached failure, the strain increased linearly and peaked. Because of the influence of expansion and compression, the strain growth rate was slowest, and the strain was smallest at measuring points R2 and R3 adjacent to the failure site.

Figure 3b indicates that the axial and circumferential strain changes were entirely different. The pipeline's axial strain increased linearly during the axial force loading stage. At this point, the intact pipeline was in the elastic axial tension stage, and the strain increase rate at each measuring point was identical. An internal pressure load was then applied, focusing on the deformation of the intact pipeline under internal pressure in the circumferential strain. The axial strain remained at a plateau stage, almost unchanged.

After 1300 s of loading and an internal pressure greater than 9.05 MPa, the intact pipeline's deformation concentrated at the burst location. The axial strains at measuring points R15 and R18, which were close to the blasting position, began to rise due to compression at the failure site and boundary constraints, with the strain being the maximum among all measuring points. The axial strain at measuring point R17 began to decrease due to the expansion of the failure site, the lowest value among all measuring points.

Verification of the calculation equation

Table 2 compares the error distributions of the 35 burst tests to demonstrate the superiority of the limit state equation in estimating failure pressure. The 35 experiments include one experiment

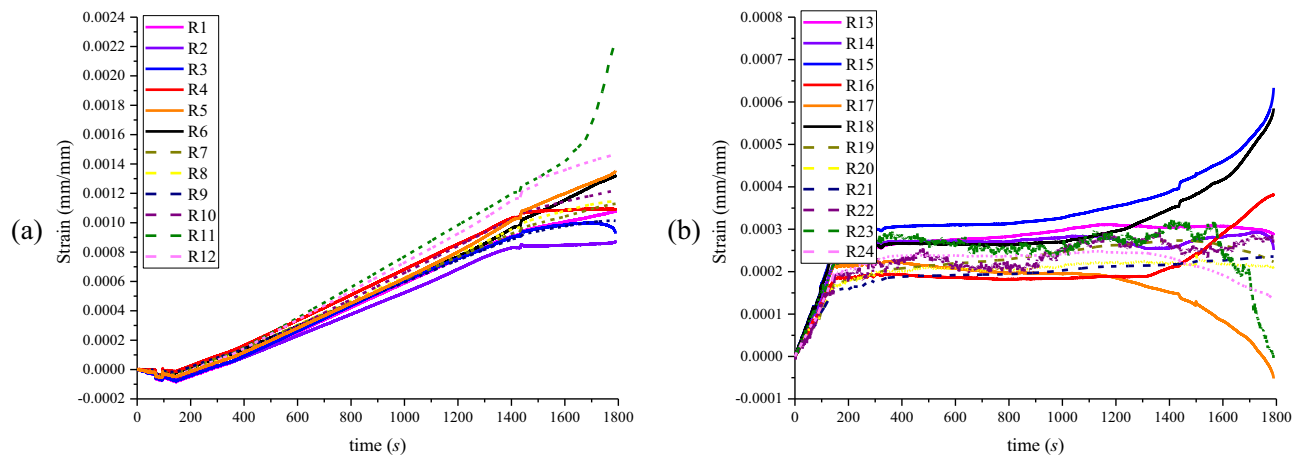


Fig. 3 | Strain curve of an intact pipeline. **a** Time series variation curves for circumferential strain at 12 measurement points (R1-R12). The axial force load was 0–147 s, and the pipeline was primarily subjected to axial tensile deformation. The circumferential strain R1-R12 generated compressive strain via Poisson's action. After the axial force loading was completed, internal pressure was applied, which significantly increased the circumferential strain. **b** Time series variation curves for axial strain at 12 measuring points (R13-R24). The pipeline's axial strain increased

linearly during the axial force loading stage. The pipeline primarily deformed along its circumference during the internal pressure loading stage. The axial strain remained stable, with a small amplitude of variation. As the internal pressure exceeded 9.05 MPa, the pipeline's deformation concentrated at the burst position. With the expansion, the axial strain at measuring points R15 and R18 near the burst location increased. The measuring point R17 at the edge of the expansion zone significantly reduced axial strain with compression.

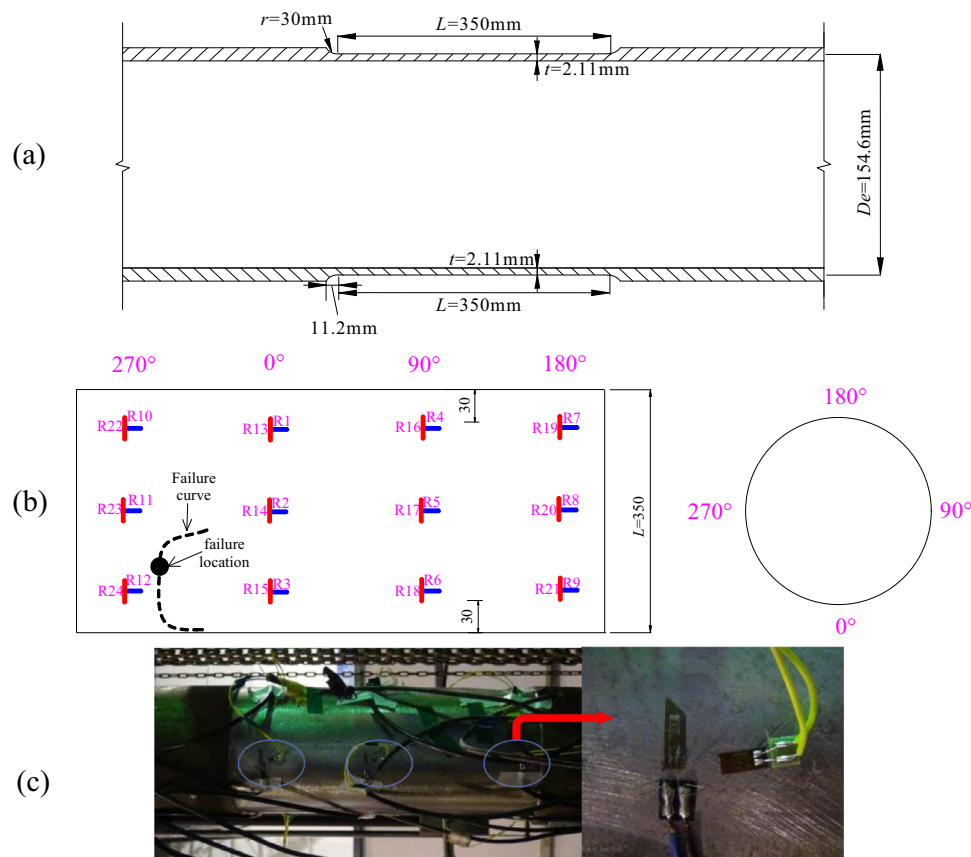


Fig. 4 | The test pipeline and the strain gauge. **a** A schematic diagram of the test pipeline (mm). The average diameter D_e of the test pipeline was 154.6 mm, the average wall thickness t was 2.11 mm, and the length L was 350 mm. The experimental pipeline ended with a circular arc transition with a radius of 30 mm and a length of 11.2 mm to prevent stress concentration. **b** Strain gauge layout in an intact pipeline section (mm). The blue marks are strain gauges for circumferential strain, while the red marks are for axial strain. At the end and middle of the experimental

pipeline, three layers of strain gauges are arranged in circumferential directions of 0°, 90°, 180°, and 270°, respectively. Therefore, strain gauges were placed in 12 different locations along the pipeline, with each location divided into axial and circumferential strain gauges. The failure occurred near the bottom of the experimental pipeline, between 270° and 0° (360°). **c** Physical diagram of the strain gauge.

illustrated in Figs. 4, 5 experiments from ref. 51, and 29 experiments from ref. 52. Specifically, it compares the error parameters of this study's proposed evaluation method with various yield criteria. It shows that the von Mises criterion was the most adaptable and stable of the four conventional yield criteria, with an average error of only 5.26%. Moreover, the standard deviation was only 0.0429, the lowest value among the four yield criteria. The Tresca yield criterion had the worst adaptability, with the highest average error and a wide range of prediction results. Accordingly, as analyzing burst failure of pipeline with complex loads, the second principal stress must be considered. The burst failure of pipelines carrying complex loads results from the first and second principal stresses acting simultaneously. In this sense, the yield criteria ASSY and TS had similar average errors and standard deviations, with ASSY (standard deviation = 0.0580) exhibiting a better applicability. The ASSY prediction results were conservative, whereas those of TS were dangerous. Between the ASSY and TS yield criteria, factor *b* in the von Mises criterion determined the extent to which the second principal stress influenced the failure stress. The von Mises criterion was more closely related to the characteristics of pipeline blasting failure under complex loads, hence the prediction results were more accurate.

To compensate for the limitations of the experimental data, FE results were used to validate the developed calculation equation. Table 3 shows the errors of the FE models. As shown in the said table, the average error of the Tresca yield criteria was lower than in Table 2. This was due to a smaller axial force ($\sum \frac{\sigma_i}{\sigma_u} = 0.3$) and a lower impact

level of the second principal stress, which reduced the Tresca criterion's error. At the same time, the error in the TS criteria increased. The average error and standard deviation for ASSY were the smallest. Meanwhile, the Tresca and von Mises yield criteria differed only slightly from the ASSY criteria, and they all exhibited good adaptability.

According to the overall distribution of errors (Tables 2 and 3), the von Mises yield criterion presented the greatest adaptability, with the lowest error (7.90%) and standard deviation (0.0955) of any yield criterion. The ASSY yield criterion exhibited the next highest applicability, while there were significant errors in the Tresca and TS yield criteria (17–18%).

Discussion

The UYC and the three-dimensional mechanical model proposed a model for assessing the burst pressure of pipelines under complex loads. The full-scale burst test clarified the pipeline's failure mode under complex loads and the applicability of various yield criteria in failure pressure assessment. The conclusions are as follows.

- (1) Since the magnitudes of the three principal stresses with complex loads differed, pipeline limit state equations likewise differed.
- (2) Circumferential stress remained a key indicator of internal pressure failure in pipelines carrying complex loads. The maximum circumferential failure strain was roughly 3.43 times the maximum axial failure strain.
- (3) This study developed a relatively accurate method for determining failure pressure based on principal stress distribution under complex loads. The von Mises yield criterion, followed by the ASSY yield criterion, exhibited good applicability in a wide range of load combinations.

Methods

This study discusses pipelines' bearing capacity under complex loads through theoretical derivation, experimentation, numerical simulation, and data analysis. First, it developed the pipeline's limit state equation using the three-dimensional stress distribution model. This equation represents a set of different yield criteria. The self-developed "Complex Load Testing Machine for Pipelines" was used to conduct failure experiments on pipelines with internal pressure and axial force. Then, this study determined the failure mode and the pipeline's internal pressure ultimate bearing capacity using the temporal variation characteristics of strain at various pipeline positions. Finally, a failure pressure database was created using the experiments described

Table 2 | The errors of each proposed evaluation method (burst test)

Index	Error with different yield criterias			
	Tresca (<i>b</i> = 0)	ASSY (<i>b</i> = 0.168)	von Mises (<i>b</i> = 0.366)	TS (<i>b</i> = 1)
min	−0.11%	−0.11%	0.16%	−0.27%
max	−59.85%	−23.90%	16.93%	35.60%
average	12.60%	7.83%	5.26%	7.80%
standard deviation	0.1278	0.0580	0.0429	0.0841

error = (*p_i* − *p_T*)/*p_T* × 100%; *P_i* is the predicted value; *P_T* denotes the test's failure pressure; average = $\sum |error|/35$; *b* is the yield criterion parameter.

Table 3 | The errors of each proposed evaluation method (FE model)

steel grade	case	error with different yield criteria			
		Tresca (<i>b</i> = 0)	ASSY (<i>b</i> = 0.168)	von Mises (<i>b</i> = 0.366)	TS (<i>b</i> = 1)
X52	C-C0.3-B0.3	−0.01%	6.16%	10.38%	16.38%
	C-C0.3-B0.05	14.27%	16.93%	19.58%	25.72%
	C-T0.3-B0.3	−14.00%	−7.37%	−0.73%	14.59%
	C-T0.3-B0.05	18.30%	8.41%	1.65%	−7.97%
	T-C0.3-B0.3	−6.37%	0.89%	8.15%	24.92%
	T-C0.3-B0.05	9.05%	13.26%	17.47%	27.20%
	T-T0.3-B0.3	−6.37%	5.43%	−9.23%	−12.53%
	T-T0.3-B0.05	9.04%	13.41%	17.48%	27.85%
min		−14.00%	−7.37%	−9.23%	−12.53%
max		18.30%	16.93%	19.58%	27.85%
average		9.68%	8.98%	10.58%	19.65%
Standard deviation		0.1138	0.0781	0.1023	0.1609

Error = (*p_i* − *p_T*)/*p_T* × 100%; *P_i* is the predicted value; *P_T* denotes the test result; average = $\sum |error|/8$; *b* is the yield criterion parameter.

in this study and other experimental and numerical model results, and the applicability of various yield criteria were compared and analyzed.

Theory of the limit state equation

The UYC^{53–55} considers the contribution of the second principal stress σ_2 to structural failure. Steel pipelines can be considered a tension-compression isotropic material. The UYC criteria may be expressed as follows:

$$C = \begin{cases} \tau_{13} + b\tau_{12}, \tau_{12} \geq \tau_{23} \\ \tau_{13} + b\tau_{23}, \tau_{12} < \tau_{23} \end{cases} \quad (3)$$

where τ_{13} , τ_{12} , and τ_{23} are the principal shear stresses, and C is a material parameter.

$$C = \frac{1+b}{2} \sigma_{UE} \quad (4)$$

where σ_{UE} is the UYC equivalent stress.

From Eqs. (3) and (4):

$$\sigma_{UE} = \begin{cases} \sigma_1 - \frac{1}{1+b}(b\sigma_2 + \sigma_3), \sigma_2 \leq \frac{\sigma_1 + \sigma_3}{2} \\ \frac{1}{1+b}(\sigma_1 + b\sigma_2) - \sigma_3, \sigma_2 > \frac{\sigma_1 + \sigma_3}{2} \end{cases} \quad (5)$$

where σ_1 , σ_2 , and σ_3 are the principal stresses, and $\sigma_1 \geq \sigma_2 \geq \sigma_3$.

The UYC is a set of various criteria, as illustrated in Supplementary Fig. 1⁵⁶. The value range of b is $0 \leq b \leq 1$.

(1) As $b = 0$, the effect of the second principal shear stress on the equivalent stress of plastic failure of the pipeline is completely ignored, and the criterion is analogous to the Tresca yield criterion.

(2) As $b = 1$, the equivalent stress of plastic failure in a pipeline is influenced by the first and second principal shear stresses, and the weights of the two stresses are equal. The yield criterion is based on twin shear stress (TS).

(3) As $0 < b < 1$, the second principal shear stress affects the equivalent stress of plastic failure in a pipeline, but its weight is lower than the first principal shear stress. For example, as $b = 1/(1 + \sqrt{3}) \approx 0.366$, the criterion approximates to the von Mises criterion; as $b = (8\sqrt{3} - 10)/23 \approx 0.168$, the criterion is the average shear stress yield criterion (ASSY).

For thin-walled pipelines ($(D_e/t) \geq 20$), Eqs. (6) and (7) can be used to calculate circumferential stress σ_h and axial stress $(\sigma_L)_p$ by pressure. Radial stress σ_r can be ignored relative to the other stresses.

$$\sigma_h = p \frac{D_e}{2t} \quad (6)$$

$$(\sigma_L)_p = \frac{\sigma_h}{2} \quad (7)$$

where D_e is the outer diameter.

Equations (8) and (9) can be used to calculate the axial stress $(\sigma_L)_{\Delta T}$ or $(\sigma_L)_{Nc}$ generated by the temperature difference ΔT or the longitudinal force N_c .

$$(\sigma_L)\Delta T = -E\lambda\Delta T \quad (8)$$

$$(\sigma_L)_{Nc} = \frac{N_c}{A} \quad (9)$$

where E is the elastic modulus (MPa), λ denotes the temperature expansion coefficient ($^{\circ}\text{C}$), ΔT represents the temperature difference ($^{\circ}\text{C}$), A is the circumferential area of the pipeline (mm^2) in which $A = \frac{\pi}{4}(D_e^2 - D_i^2)$, and D_i denotes the inner diameter.

The axial stress $(\sigma_L)_{Mb}$ generated by the bending moment M_b is given by Eq. (10).

$$(\sigma_L)_{Mb} = \pm \frac{M_b D_e}{I} \quad (10)$$

where I is cross sectional moment of inertia in which $I = \frac{\pi}{64}(D_e^4 - D_i^4)$.

The total axial stress σ_L is the sum of $(\sigma_L)_p$ and the stress $\Sigma(\sigma_L)$ generated by bending moment, axial force, and others.

$$\sigma_L = (\sigma_L)_p \pm \Sigma(\sigma_L) \quad (11)$$

For the burst failure of a pipeline, σ_{UE} can be taken as σ_u ⁵⁷. The properties of axial stress allow the solution of the limit state equation in the following situations:

- As the additional loadings are positive (tensile), and $\sigma_1 = \sigma_L$, $\sigma_2 = \sigma_h$, $\sigma_3 = 0$.
- If $\sigma_2 \leq \frac{\sigma_1 + \sigma_3}{2}$, according to Eq. (5):

$$\sigma_{UE} = \sigma_1 - \frac{1}{1+b}(b\sigma_2 + \sigma_3) = \sigma_u \quad (12)$$

$$\sigma_L = (\sigma_L)_p + \Sigma(\sigma_L) \quad (13)$$

$$\sigma_u = p_0 \frac{D_e}{2t} \quad (14)$$

where p_0 is the intact pipeline's burst pressure.

Substituting Eqs. (13) and (6) into Eq. (12):

$$(\sigma_L)_p + \Sigma(\sigma_L) - \frac{b}{1+b} p \frac{D_e}{2t} = \sigma_u \quad (15)$$

$$\frac{(\sigma_L)_p}{\sigma_u} + \frac{\Sigma(\sigma_L)}{\sigma_u} - \frac{b}{1+b} \frac{p \frac{D_e}{2t}}{\sigma_u} = 1 \quad (16)$$

Substituting Eqs. (6), (7), and (14) into Eq. (16):

$$\frac{\frac{1}{2} p \frac{D_e}{2t}}{p_0 \frac{D_e}{2t}} + \frac{\Sigma(\sigma_L)}{\sigma_u} - \frac{b}{1+b} \frac{p \frac{D_e}{2t}}{p_0 \frac{D_e}{2t}} = 1 \quad (17)$$

In this case, the limit state equation is defined as:

$$\left(\frac{1}{2} - \frac{b}{1+b} \right) \frac{p}{p_0} + \frac{\Sigma(\sigma_L)}{\sigma_u} = 1 \quad (18)$$

- If $\sigma_2 > \frac{\sigma_1 + \sigma_3}{2}$, according to Eq. (5):

$$\sigma_{UE} = \frac{1}{1+b}(\sigma_1 + b\sigma_2) - \sigma_3 = \sigma_u \quad (19)$$

Substituting Eqs. (13) and (6) into Eq. (19):

$$\frac{1}{1+b} \left((\sigma_L)_p + \Sigma(\sigma_L) + b p \frac{D_e}{2t} \right) = \sigma_u \quad (20)$$

$$\frac{1}{1+b} \left(\frac{(\sigma_L)_p}{\sigma_u} + \frac{\Sigma(\sigma_L)}{\sigma_u} + b \frac{p \frac{D_e}{2t}}{\sigma_u} \right) = 1 \quad (21)$$

Substituting Eqs. (6), (7), and (14) into Eq. (21):

$$\frac{1}{1+b} \left(\frac{\frac{1}{2} p \frac{D_e}{2t}}{p_0 \frac{D_e}{2t}} + \frac{\Sigma(\sigma_L)}{\sigma_u} + b \frac{p \frac{D_e}{2t}}{p_0 \frac{D_e}{2t}} \right) = 1 \quad (22)$$

Table 4 | Data of burst tests

literature Sources	test No.	diameter (mm)	grade	D/t	axial stress (MPa)	yield strength (MPa)	tensile Strength (MPa)
Paslay et al. ⁵³	13	88.9	L80	14.5	348.79247	695.201	753.766
	16	88.9	L80	18.0	586.66283	695.201	753.766
	17	88.9	L80	18.6	638.14491	695.201	753.766
	18	177.8	K55	26.7	454.31971	465.764	737.23
	19	196.85	Q125	18.1	884.73801	905.346	993.538
Lasebikan et al. ^{54a}	22 °C-1	8	125		450	969	1063
	22 °C-2				450		
	22 °C-3				460		
	22 °C-4				550		
	22 °C-5				540		
	22 °C-6				650		
	22 °C-7				655		
	22 °C-8				665		
	22 °C-9				750		
	22 °C-10				751		
	22 °C-11				740		
	22 °C-12				750		
	90 °C-1				400	881	948
	90 °C-2				410		
	90 °C-3				410		
	90 °C-4				550		
	90 °C-5				551		
	90 °C-6				650		
	110 °C-1				400	851	935
	110 °C-2				400		
	110 °C-3				400		
	110 °C-4				550		
	110 °C-5				545		
	110 °C-6				550		
	160 °C-1				400	821	888
	160 °C-2				400		
	160 °C-3				550		
	160 °C-4				550		
	160 °C-5				650		

*Note: Data were obtained from the reference literature's charts; D and t represent the diameter and the wall thickness, respectively.

In this case, the limit state equation is defined as:

$$\left(\frac{1}{2(1+b)} + \frac{b}{b+1}\right) \frac{p}{p_0} + \frac{1}{1+b} \frac{\sum(\sigma_L)}{\sigma_u} = 1 \tag{23}$$

In this case, the limit state equation is defined as:

$$\left(1 - \frac{1}{2(1+b)}\right) \frac{p}{p_0} - \frac{1}{1+b} \frac{\sum(\sigma_L)}{\sigma_u} = 1 \tag{26}$$

2. As the additional loadings are positive (tensile), and $\sigma_1 = \sigma_h, \sigma_2 = \sigma_L, \sigma_3 = 0$, i.e., $\sigma_2 > \frac{\sigma_1 + \sigma_3}{2}$, the limit state equation is defined as:

$$\frac{1}{1+b} \left(1 + \frac{b}{2}\right) \frac{p}{p_0} + \frac{b}{1+b} \frac{\sum(\sigma_L)}{\sigma_u} = 1 \tag{24}$$

The limit state equation is defined as:

$$\left(\frac{1}{b+1} - \frac{1}{2}\right) \frac{p}{p_0} + \frac{\sum(\sigma_L)}{\sigma_u} = 1 \tag{27}$$

3. As the additional loadings are negative (compressive), and $\sigma_1 = \sigma_h, \sigma_2 = 0, \sigma_3 = \sigma_L$.

(1) If $\sigma_2 \leq \frac{\sigma_1 + \sigma_3}{2}$

$$\sigma_L = (\sigma_L)p - \sum(\sigma_L) \tag{25}$$

4. As the additional loadings are negative (compressive), and $\sigma_1 = \sigma_h, \sigma_2 = \sigma_L, \sigma_3 = 0$, i.e., $\sigma_2 \leq \frac{\sigma_1 + \sigma_3}{2}$, the limit state equation is defined as:

$$\left(1 - \frac{b}{2(1+b)}\right) \frac{p}{p_0} + \frac{b}{1+b} \frac{\sum(\sigma_L)}{\sigma_u} = 1 \tag{28}$$

Full-scale burst test

A full-scale test with axial force and internal pressure was carried out to examine the burst model of intact pipelines under various loads. Supplementary Figs. 2 and 3 show the processing of experimental pipelines. Supplementary Fig. 4 and Supplementary Note 1 describe the experimental setup and procedure. The overall wall thickness reduction treatment was performed in the middle of the pipeline to produce an intact, defect-free section. Circular arcs cross both processed and unprocessed parts to prevent stress concentration. Fig. 4a depicts the axial interface of the processed pipeline.

The transition arc had a radius of 30 mm and a length of 11.2 mm. The pipeline's strength grade was Q235, a Chinese standard steel grade. It is a carbon structural steel with a yield strength standard of 235 MPa. Q235 steel is widely used in construction, bridges, pipelines, and other structural applications because of its good weldability, machinability, and strength. The experimental pipeline's measured yield and tensile strength were 280 and 415.5 MPa, respectively.

The primary cause of axial force during the operation of buried pipelines, among other factors, is temperature differential. In this study, the temperature difference was set to 27 °C. Because temperature-induced axial force is challenging to release via pipeline axial elongation, the temperature difference causes the pipeline to generate axial force, which can be estimated using the following equation:

$$N_c = -AE\lambda\Delta T \quad (29)$$

Table 5 | The errors of the FE model

steel grade	case	failure pressure in the test (MPa)	failure pressure with FE model (MPa)	error
Q235	test in the paper	11.69	11.70	0.09%
L80	13	115.48	111.67	−3.30%
L80	16	64.08	68.68	7.18%
L80	17	50.64	50.66	0.03%
K55	18	54.84	57.37	4.62%
Q125	19	63.39	61.20	−3.45%
min		−3.45%		
max		7.18%		
average		3.11%		
Standard deviation		0.0427		

Error = $(p_{FE} - p_T)/p_T \times 100\%$; p_{FE} is the predicted value; p_T denotes the failure pressure of the test; average = $\sum |error|/6$. The “residual wall thickness stress criterion” determined the failure pressure of the pipelines^{5,59}.

where N_c is a negative value and represents the axial compression force (N). The calculated value of N_c was 68 kN, which was used in the experiment.

Fig. 4b, c present the arrangement mode of the strain gauge for the burst test of intact pipelines. The strain gauges were arranged in four directions along the pipeline's axial circular section, namely 0°, 90°, 180°, and 270°. Each direction had circumferential and axial strains at both ends and the middle to monitor the strain in the intact pipeline.

Data analysis

Table 4 displays the full-scale burst test data from refs. 51,52, which included axial force and internal pressure. Supplementary Table 1 shows detailed predicted values and error data.

Numerical simulation

The FE model was chosen for validation under the following criteria:

(1) The burst test lacked data at $0.2 < \frac{\sum(\sigma_t)}{\sigma_u} < 0.4$; thus, the value of $\frac{\sum(\sigma_t)}{\sigma_u}$ was taken as 0.3.

(2) The burst test lacked axial compression data; thus, axial force data was supplemented with compressive stress.

(3) The experiment lacked bending moment load; thus, pipeline burst data with “bending moment-axial force-internal pressure” was added.

In this case, ABAQUS created a geometric model, and the corresponding finite element model was built with the three-dimensional solid unit C3D8R. The pipeline was divided into four layers of units in the thickness direction, 48 units in the circumferential direction, and 88 units in the axial direction. Reference points were established at both pipeline ends, and rigid beam constraints were utilized to connect the reference points to the pipeline end nodes. The analyzed model is depicted in Supplementary Fig. 5.

The bending moment (M_b) and the axial force (N_c) were applied to the designated reference node while gradually increasing the internal pressure on the inner surface nodes until the pipe burst.

The nonlinear arc-length method algorithm was utilized to solve the finite element model. The simulation applied a pipeline material with isotropic hardening plasticity. This study used the well-known Ramberg-Osgood model to represent the stress-strain relationship accurately.

The burst data in Table 4 was used to validate the model, and the results are shown in Table 5. The average error was 3.11%, which falls within the acceptable range. Thus, the model's accuracy was verified.

Table 6 | Results of finite element model

test No.	diameter (mm)	grade	yield strength (MPa)	tensile Strength (MPa)	t	axial Stress (MPa)	bend moment (N-mm)	failure pressure (MPa)
C-C0.3-B0.3	914.4	X52	413	545	9.525	$-0.3\sigma_u$	$0.3M_0$	9.11
C-C0.3-B0.05						$-0.3\sigma_u$	$0.05M_0$	9.94
C-T0.3-B0.3						$0.3\sigma_u$	$0.3M_0$	13.20
C-T0.3-B0.05						$0.3\sigma_u$	$0.05M_0$	14.39
T-C0.3-B0.3						$-0.3\sigma_u$	$0.3M_0$	12.13
T-C0.3-B0.05						$-0.3\sigma_u$	$0.05M_0$	10.41
T-T0.3-B0.3						$0.3\sigma_u$	$0.3M_0$	12.13
T-T0.3-B0.05						$0.3\sigma_u$	$0.05M_0$	10.41

“-” represents the compressive stress; M_0 is the ultimate elastic buckling moment, in which $M_0 = D^2\sigma_y^{60.61}$; “C/T-C0.3/T0.3-B0.3/B0.05” means “failure pressure on the Compression side or Tensile side caused by bending moment,” “Compression or Tensile stress is $0.3\sigma_u$,” and “Bending moment is $0.3M_0$ or $0.05M_0$.”

The size and strength data of X52 from the Yi Shuai and Xiao Zhang models were used for analysis³⁸. The reasons for utilizing the said data are as follows:

- (1) In the absence of medium-strength pipeline data in the burst test, X52 steel was chosen as a representative sample for analysis.
- (2) Due to a lack of data on the large diameter-to-thickness ratio in the test (the burst test in Table 3 has a ratio of 14.5–73.0), $D/t = 96$ was chosen as a representative value. Table 6 shows the specific FE model.

Data availability

Source data is available as Source Data file. It also has been deposited in the Zenodo database at <https://doi.org/10.5281/zenodo.11118137>. Source data are provided with this paper.

References

1. Wang, Q. et al. Evolution of corrosion prediction models for oil and gas pipelines: From empirical-driven to data-driven. *Eng. Fail. Anal.* **146**, 107097 (2023).
2. Wuyi, W., Xiaoyi, C., Boran, Z. & Jijian, L. Transient Simulation and Diagnosis of Partial Blockage in Long-Distance Water Supply Pipeline Systems. *J. Pipeline Syst. Eng. Practice*. **12**, (2021).
3. Guojin, Q. et al. A hybrid machine learning model for predicting crater width formed by explosions of natural gas pipelines. *J. Loss Prevent. Proc.* **82**, 104994 (2023).
4. Zhu, X. K. A comparative study of burst failure models for assessing remaining strength of corroded pipelines. *J. Pipeline Sci. Eng.* **1**, 36–50 (2021).
5. Sun, M., Zhao, H., Li, X., Liu, J. & Xu, Z. New evaluation method of failure pressure of steel pipeline with irregular-shaped defect. *Appl. Ocean Res.* **110**, 102601 (2021).
6. Sun, M., Zhao, H., Li, X., Liu, J. & Xu, Z. A new evaluation method for burst pressure of pipeline with colonies of circumferentially aligned defects. *Ocean Eng.* **222**, 108628 (2021).
7. Alliance, A. L. Guidelines for the design of buried steel pipe. *American Society of Civil Engineers*. America: American Society of Civil Engineers; 2001.
8. API. *Specification for Line Pipes*, 41st edition edn. (API Specification 5L, Washington, 2000).
9. API. *Design, Construction, Operation, and Maintenance of Offshore Hydrocarbon Pipelines (Limit State Design)*. (American Petroleum Institute, Washington, 1999).
10. Kim, H. S. & Kim, W. S. Analysis of Stresses on Buried Natural Gas Pipeline Subjected to Ground Subsidence. *Proc. Int. Pipeline Conference*. Alberta, Canada; 1998.
11. Sun, M., Chen, Y., Zhao, H. & Li, X. Analysis of the impact factor of burst capacity models for defect-free pipelines. *Int. J. Pres. Ves. Pip.* **200**, 104805 (2022).
12. Taylor, N., Clubb, G. & Matheson, I. The effect of bending and axial compression on pipeline burst capacity. SPE Offshore Europe Conference and Exhibition; Aberdeen, Scotland, UK: OnePetro; 2015. 175464 (2015).
13. Dewanbabe, H. & Das, S. Structural behavior of corroded steel pipes subject to axial compression and internal pressure: Experimental study. *J. Struct. Eng.* **139**, 57–65 (2013).
14. Lo, M., Karuppanan, S. & Ovinis, M. Failure pressure prediction of a corroded pipeline with longitudinally interacting corrosion defects subjected to combined loadings using FEM and ANN. *J. Marine Sci. Eng.* **9**, 281 (2021).
15. Couque, H. R., Smith, M. Q., Grigory, S. C. & Kanninen, M. F. The development of methodologies for evaluating the integrity of corroded pipelines under combined loading. Part 1: Experimental testing and numerical simulations. *Energy Week '96: American Society of Mechanical Engineers and American Petroleum Institute energy week conference and exhibition*. Houston, TX (United States). 58–66 (1996).
16. Couque, H. R., Smith, M. Q., Grigory, S. C. & Kanninen, M. F. The development of methodologies for evaluating the integrity of corroded pipelines under combined loading. Part 2: Engineering model and PC program development. *Energy Week '96: American Society of Mechanical Engineers and American Petroleum Institute energy week conference and exhibition*. Houston, TX (United States). 67–76 (1996).
17. Smith, M. Q. & Grigory, S. C. New Procedures for the Residual Strength Assessment of Corroded Pipe Subjected to Combined Loads. 1st International Pipeline Conference; Calgary, Alberta, Canada; 1996. 387–400 (1996).
18. Smith, M. Q., Nicoletta, D. P. & Waldhart, C. J. Full-scale wrinkling tests and analyses of large diameter corroded pipes. *2nd International Pipeline Conference*. Calgary, Alberta, Canada: American Society of Mechanical Engineers. pp. 543–551 (1998).
19. Wang, W., Smith, M. Q., Popelar, C. H. & Maple, J. A. A new rupture prediction model for corroded pipelines under combined loadings. *2nd International Pipeline Conference*. Calgary, Alberta, Canada: American Society of Mechanical Engineers. 563–572 (1998).
20. Roy et al. The development of methodologies for determining the residual strength of corroded line pipe under combined loading. *The 50th NACE Annual Conference and Corrosion Show (CORROSION'95)*. Orlando, FL (United States). 21–22 (1995).
21. Smith, M. Q. & Waldhart, C. J. Combined loading tests of large diameter corroded pipelines. *3rd International Pipeline Conference*. Calgary, Alberta, Canada: American Society of Mechanical Engineers. V2T-V6T (2000).
22. Roy, S. Numerical Simulations of Full-Scale Corroded Pipe Tests with Combined Loading. *J. Press. Vessel Tech.* **119**, 457–466 (1997).
23. Sigurdsson, G., Cramer, E. H., Bjørnøy, O. H., Fu, B. & Ritchie, D. Background to DNV RP-F101 Corroded pipelines. The 18th international conference on offshore mechanics and arctic engineering. 1999; Newfoundland, Canada: American Society of Mechanical Engineers (1999).
24. Bjørnøy, O. H., Sigurdsson, G., Cramer, E. H., Fu, B. & Ritchie, D. Introduction to DNV RP-F101 Corroded Pipelines. The 19th International Conference on Offshore Mechanics and Arctic Engineering. 1999; Newfoundland, Canada: American Society of Mechanical Engineers (1999).
25. Bjørnøy, O. H., Sigurdsson, G. & Marley, M. J. Background and development of DNV-RP-F101 corroded pipelines. *The Eleventh International Offshore and Polar Engineering Conference*. Stavanger, Norway: OnePetro; pp. 1–139 (2001).
26. Bjørnøy, O. H., Cramer, E. H. & Sigurdsson, G. Probabilistic Calibrated Design Equation For Burst Strength Assessment of Corroded Pipes. *The Seventh International Offshore and Polar Engineering Conference*. Honolulu, Hawaii, USA: OnePetro. 160–166 (1997).
27. Bjørnøy, O. H., Sigurdsson, G. & Cramer, E. Residual strength of corroded pipelines, DNV test results. *The Tenth International Offshore and Polar Engineering Conference* (pp. 140. OnePetro, Seattle, Washington, USA, 2000).
28. Bjørnøy, O. H. & Marley, M. J. Assessment of corroded pipelines: past, present and future. 11th International Offshore and Polar Engineering Conference. 2001 2001-01-01; Stavanger, Norway: International Society of Offshore and Polar Engineers. p. 1–138 (2001).
29. Mondal, B. C. & Dhar, A. S. Burst pressure of corroded pipelines considering combined axial forces and bending moments. *Eng. Struct.* **186**, 43–51 (2019).

30. Pengcheng, Z., Jian, S., Yu, T. & Kui, X. U. Impact of axial stress on ultimate internal pressure of corroded pipelines. *China Safety Sci J* **29**, 70–75 (2019).
31. Zhou, H., Wang, Y., Stephens, M., Bergman, J. & Nanney, S. Burst pressure of pipelines with corrosion anomalies under high longitudinal strains. 12th International Pipeline Conference. 2018; Calgary, Alberta, Canada: American Society of Mechanical Engineers. V2T-V6T (2018).
32. Chen, Z., Wang, W., Yang, H., Yan, S. & Jin, Z. On the effect of long corrosion defect and axial tension on the burst pressure of subsea pipelines. *Appl. Ocean Res.* **111**, 102637 (2021).
33. Chauhan, V. & Swankie, T. Guidance for assessing the remaining strength of corroded pipelines. Washington, DC, USA: US Department of Transportation: Pipeline and Hazardous Materials Safety Administration. Report No.: Report No. 9492, Project #153M (2015).
34. Liu, J., Chauhan, V., Ng, P., Wheat, S. & Hughes, C. Remaining strength of corroded pipe under secondary (biaxial) loading. Washington, DC, USA: US Department of Transportation: GL Industrial Services UK Ltd. Report No.: Report No. R9068, Project # 153J (2009).
35. Heitzer, M. Plastic limit loads of defective pipes under combined internal pressure and axial tension. *Int. J. Mech. Sci.* **44**, 1219–1224 (2002).
36. Benjamin, A. C. Prediction of the failure pressure of corroded pipelines subjected to a longitudinal compressive force superimposed to the pressure loading. 7th International Pipeline Conference. Calgary, Alberta, Canada. 179–189 (2008).
37. Bruère, V. M. et al. Failure pressure prediction of corroded pipes under combined internal pressure and axial compressive force. *J. Braz. Soc. Mech. Sci.* **41**, 1–10 (2019).
38. Arumugam, T., Mohamad Rosli, M. K. A., Karuppanan, S., Ovinis, M. & Lo, M. Burst capacity analysis of pipeline with multiple longitudinally aligned interacting corrosion defects subjected to internal pressure and axial compressive stress. *SN Appl. Sci.* **2**, 1–11 (2020).
39. Zhang, S., Zhou, W. & Zhang, S. Development of a burst capacity model for corroded pipelines under internal pressure and axial compression using artificial neural network. 13th International Pipeline Conference. Virtual, Online: American Society of Mechanical Engineers. V1T-V3T (2020).
40. Shuai, Y., Wang, X. & Cheng, Y. F. Modeling of local buckling of corroded X80 gas pipeline under axial compression loading. *J. Nat. Gas Sci. Eng.* **81**, 103472 (2020).
41. Konosu, S. & Mukaimachi, N. Plastic collapse assessment procedure for vessel with local thin area simultaneously subjected to internal pressure and external bending moment. *J. Pressure Vessel Technol.* **130**, 11207 (2008).
42. Mohd, M. H., Lee, B. J., Cui, Y. & Paik, J. K. Residual strength of corroded subsea pipelines subject to combined internal pressure and bending moment. *Ships Offshore Struct.* **10**, 554–564 (2015).
43. Chegeni, B., Jayasuriya, S. & Das, S. Effect of corrosion on thin-walled pipes under combined internal pressure and bending. *Thin Wall. Struct.* **143**, 106218 (2019).
44. Gao, J., Peng, Z., Li, X., Zhou, J. & Zhou, W. Bending capacity of corroded pipeline subjected to internal pressure and axial loadings. 37th International Conference on Offshore Mechanics and Arctic Engineering. Madrid, Spain: American Society of Mechanical Engineers. V2T-V3T (2018).
45. Bai, Y. & Hauch, S. Collapse capacity of corroded pipes under combined pressure, longitudinal force and bending. *Int. J. Offshore Polar.* **11**, 1–11 (2001).
46. Tian, X., Zhang, H. & Lu, M. Effect of axial force and bending moment on the limit internal pressure of dented pipelines. *Eng. Fail. Anal.* **106**, 104168 (2019).
47. Vitali, L., Bruschi, R., Mork, K. J., Levold, E. & Verley, R. Hotpipe project: Capacity of pipes subject to internal pressure, axial force and bending moment. *The Ninth International Offshore and Polar Engineering Conference*. Brest, France: OnePetro (1999).
48. Ozkan, I. F. & Mohareb, M. Moment resistance of steel pipes subjected to combined loads. *Int. J. Pres. Ves. Pip.* **86**, 252–264 (2009).
49. Ozkan, I. F. & Mohareb, M. Testing and analysis of steel pipes under bending, tension, and internal pressure. *J. Struct. Eng.* **135**, 187–197 (2009).
50. Agarwal, R. Texas A&M University. *Tube bending with axial pull and internal pressure*, (2004).
51. Paslay, P. R., Cernocky, E. P. & Wink, R. Burst pressure prediction of thin-walled, ductile tubulars subjected to axial load. SPE Applied Technology Workshop on Risk Based Design of Well Casing and Tubing; Woodlands, Texas: Society of Petroleum Engineers; 1998. 48327 (1998).
52. Lasebikan, B. A. & Akisanya, A. R. Burst pressure of super duplex stainless steel pipes subject to combined axial tension, internal pressure and elevated temperature. *Int. J. Pres. Ves. Pip.* **119**, 62–68 (2014).
53. Yu, M. H. & He, L. N. *A new model and theory on yield and failure of materials under the complex stress state*. (Elsevier, 1992).
54. Fan, S. C., Yu, M. & Yang, S. On the unification of yield criteria. *J. Appl. Mech.-T. ASME*. **68**, 341–343 (2001).
55. Yu, M. Advances in strength theories for materials under complex stress state in the 20th century. *Appl. Mech. Rev.* **55**, 169–218 (2002).
56. Wang, L. & Zhang, Y. Plastic collapse analysis of thin-walled pipes based on unified yield criterion. *Int. J. Mech. Sci.* **53**, 348–354 (2011).
57. Sun, M., Li, X. & Liu, J. Determination of Folias factor for failure pressure of corroded pipeline. *J. Press. Vess.-T. ASME*. **142**, 31802 (2020).
58. Shuai, Y., Zhang, X., Feng, C., Han, J. & Cheng, Y. F. A novel model for prediction of burst capacity of corroded pipelines subjected to combined loads of bending moment and axial compression. *Int. J. Pres. Ves. Pip.* **196**, 104621 (2022).
59. Sun, M., Fang, H., Du, X., Wang, W. & Li, X. Study on Evaluation Method of Failure Pressure for Pipeline with Axially Adjacent Defects. *China Ocean Eng* **37**, 598–612 (2023).
60. Iflefel, I. B., Moffat, D. G. & Mistry, J. The interaction of pressure and bending on a dented pipe. *Int. J. Pres. Ves. Pip.* **82**, 761–769 (2005).
61. Zhang, X. Y. Investigation on Ultimate Load Capacity and Failure Mechanism of Corroded Submarine [D]. *Zhejiang University* (2013).

Acknowledgements

This project is supported by Research Projects in Henan Province (23A560013), the National Key R&D Program of the “14th Five-Year Plan” (2022YFC3801000), the Henan Provincial Youth Science Foundation (232300421328), the Excellent Youth Innovation Research Group Project (242300421001), and the Henan Province University Science and Technology Innovation Team (23IRTSTHN004).

Author contributions

S.M. performed data analysis, developed finite element models, solved theoretical solutions to limit state equations, and wrote the manuscript. F.H., W.N., and D.X. conducted experimental operations and data collection. Z.H. arranged the manuscript’s language. Z.K. carried out drawing-related tasks.

Competing interests

The authors declare no competing interests.

Additional information

Supplementary information The online version contains supplementary material available at <https://doi.org/10.1038/s41467-024-48688-1>.

Correspondence and requests for materials should be addressed to Hong-yuan Fang.

Peer review information *Nature Communications* thanks Zhanfeng Chen and the other, anonymous, reviewer(s) for their contribution to the peer review of this work. A peer review file is available.

Reprints and permissions information is available at <http://www.nature.com/reprints>

Publisher's note Springer Nature remains neutral with regard to jurisdictional claims in published maps and institutional affiliations.

Open Access This article is licensed under a Creative Commons Attribution 4.0 International License, which permits use, sharing, adaptation, distribution and reproduction in any medium or format, as long as you give appropriate credit to the original author(s) and the source, provide a link to the Creative Commons licence, and indicate if changes were made. The images or other third party material in this article are included in the article's Creative Commons licence, unless indicated otherwise in a credit line to the material. If material is not included in the article's Creative Commons licence and your intended use is not permitted by statutory regulation or exceeds the permitted use, you will need to obtain permission directly from the copyright holder. To view a copy of this licence, visit <http://creativecommons.org/licenses/by/4.0/>.

© The Author(s) 2024